Journal of Materials Chemistry C

ROYAL SOCIETY OF CHEMISTRY

PAPER

View Article Online
View Journal | View Issue

Cite this: J. Mater. Chem. C, 2024, 12, 18282

A facile membraneless method for detecting alkali-metal cations using organic electrochemical transistors†

Waner He, ‡[a] Yurika Kashino,‡[a] Naoya Nozaki,[a] Joost Kimpel, [b] Hidetoshi Matsumoto, [a] Yuhei Hayamizu [a] and Tsuyoshi Michinobu *[a]

Received 17th July 2024,
Accepted 2nd September 2024

DOI: 10.1039/d4tc03047h

rsc.li/materials-c

Organic electrochemical transistors (OECTs) have garnered significant attention due to their exceptional capability to efficiently monitor biological signals, making them an ideal platform for bio-signal detection. Many recent research studies have focused on detecting alkali-metal cations, such as the key cellular messengers of sodium (Na^+) and potassium (K^+) ions. We now report a straightforward and effective method for fabricating membraneless ion-selective OECTs (IS-OECTs) by directly incorporating crown ethers, specifically 18-crown-6 (18C6) and 15-crown-5 (15C5) ethers, into a polymer matrix of p(g2T-TT), a conjugated polymer bearing glycol side chains. The resulting IS-OECTs demonstrated good sensitivity and a low limit of detection for both Na^+ and K^+ ions. Importantly, stability tests revealed that 15C5-mixed polymer OECTs show no degradation over 450 continuous cycles in a NaCl aqueous solution, underscoring the excellent retention performance. This study not only provides a facile and efficient approach for the development of ion detection systems based on OECTs but also opens new avenues for advancing bioelectronic devices in future research endeavors.

1. Introduction

Recently, organic electrochemical transistors (OECTs) have attracted considerable attention due to their unique ability to convert ionic signals into electronic responses, making them highly suitable for diverse sensing applications such as biomedical diagnostics, environmental monitoring, and ion-selective sensing devices.[1–5] The fundamental principle of OECTs involves modulating channel conductivity through the interaction between the gate electrode and ions in an electrolyte. This interaction subsequently affects the charge carrier density within the organic semiconductor channel.[6–9] This intrinsic coupling of ionic and electronic processes allows for exceptional sensitivity and selectivity, even under low operating voltages, particularly in aqueous environments. One of the OECT applications is ion-selective OECTs (IS-OECTs), which monitor biologically relevant ions, such as Na^+, K^+, Ca^{2+}, and Cl^-. These ions are vital for regulating nerve, muscle, and other signal activities in humans.[10–13] Previous studies have employed IS-OECT sensors in conjunction with ion-selective membranes (ISMs).[14,15] In these cases, the selectivity of ion sensors relies on the ionophores in a plasticized polymer matrix within ISM layers.[16] Ionophores selectively and reversibly interact with target ions to form supramolecular complexes, thereby ensuring ion selectivity. For instance, Han *et al.* developed a high-performance IS-OECT with a super-Nernstian sensitivity (85 mV dec^{-1}) and a high current sensitivity (224 μA dec^{-1}) for Na^+ detection by using a polyelectrolyte film between the ISM and the channel layer.[17] In 2022, Li *et al.* enhanced the performance of an OECT by incorporating biocompatible ionic liquid [MTEOA][$MeOSO_3$] into poly(3,4-ethylenedioxythiophene):poly(4-styrenesulfonate) (PEDOT:PSS) as channel materials, achieving a high μC^* (the figure of merit of the material is defined by the product of the charge-carrier mobility μ and volumetric capacitance C^* in OECTs) of approximately 283.80 F cm^{-1} V^{-1} s^{-1}. Subsequently, ISMs were integrated into OECTs and demonstrated their capability to monitor electrophysiological events of Na^+ and K^+ ions.[18] Recently, Shi *et al.* reported a stable n-type OECT device using a C_{60} derivative with *N*,*N*,*N*-trimethyl-1-(2,3,4-tris(2-(2-methoxyethoxy)ethoxy)phenyl) methanaminium monoadduct ($PrC_{60}MA$)

[a] Department of Materials Science and Engineering, Tokyo Institute of Technology, 2-12-1 Ookayama, Meguro-ku, Tokyo 152-8552, Japan. E-mail: michinobu.t.aa@m.titech.ac.jp
[b] Department of Chemistry and Chemical Engineering, Chalmers University of Technology, 41296 Göteborg, Sweden

† Electronic supplementary information (ESI) available. See DOI: https://doi.org/10.1039/d4tc03047h

‡ These authors contributed equally.

and also introduced a selective membrane layer, enhancing the detection selectivity for Na^+ and K^+.[19]

Although many IS-OECTs demonstrated high-performance sensing properties by designing and synthesizing complicated organic semiconductors, the preparation of such ISMs on miniaturized surfaces is an arduous and costly process. Additionally, ISM implantation can lead to issues such as potential drifts due to weak membrane adhesion to the sensor surface, affecting the device readouts.[20] Therefore, developing functional single-component electronic materials, membraneless IS-OECTs, would simplify the fabrication process whilst not compromising sensor stability. This design strategy has been successfully employed by Tseng *et al.*, who showed an electrical analysis method using membraneless ion-selective PEDOT:PSS-based OECTs. Specifically, a two-PEDOT:PSS-electrode potentiostat in a microelectrode array was employed for impedance analysis to independently determine ion concentration and ion species in the range from 1 to 100 mM.[21] Given the supramolecular interactions between crown ethers and metal cations, Inal *et al.* developed a membrane-free method for detecting metal cations using the single-component conjugated polymers (CPs) functionalized with crown ether units as the gate electrodes. Subsequently, these can be used in both the recognition of a particular cation and the signal-transduction process.[22,23] Although there is a noticeable progress in the ion detection by membraneless IS-OECTs, it remains underreported and faces numerous challenges, including device stability, low sensitivity, and material selection. The membraneless, highly selective, crown ether tethered CPs by Inal *et al.* inspired us to combine crown ether units with IS-OECTs. Unlike their high-cost approach which requires CPs to be functionalized with crown ether, compounding commercially available crown ethers with the well-reported conjugated polymer named poly(2-(3,3′-bis(2-(2-(2-methoxyethoxy)ethoxy)ethoxy)-[2,2′-bithiophen]-5-yl)-thieno[3,2*b*]thiophene) (p(g2T-TT)), a simple and cost-effective method to IS-OECT active layers is achieved. The p(g2T-TT) was first synthesized by Giovannitti *et al.* in 2016, featuring hydrophilic chains, for use in OECTs. Notably, the OECT based on such a polythiophene with glycolated side chains exhibited better transconductance values than PEDOT:PSS-based OECTs of the same geometry.[24] Since this finding, research interest in employing p(g2T-TT) and other glycolated organic semiconductors for OECT applications has markedly escalated among scholars.[25,26]

In this study, we added 15-crown-5 (15C5) and 18-crown-6 (18C6) ethers into the p(g2T-TT) semiconducting polymer as a hybrid active channel layer to develop membraneless IS-OECTs. The choice of these specific crown ethers was motivated by their known affinities for Na^+ and K^+ ions, respectively.[22] Compared to the pristine p(g2T-TT), it is demonstrated that integrating these crown ethers into the polymer matrix in OECTs not only significantly enhances the ion selectivity for Na^+ and K^+ ions but also achieves good stability and improved sensitivity. Our findings underscore the potential of simple ionophore-mixed material systems for a wide range of ion-detective sensor applications.

2. Results and discussion

2.1 Optimization and characterization of polymer films

Semiconducting polymer p(g2T-TT) was synthesized as reported in the literature (Scheme S1, ESI†).[24] Before evaluation of the device, microstructure of the as-cast and annealed polymer and polymer:crown ether mixed films were studied. This is necessary since annealing facilitates polymer chain mobility, leading to improved crystallinity and better device performance. First, the microstructures of the p(g2T-TT) polymer and p(g2T-TT) with 1 wt% crown ether blend films were characterized. The two-dimensional grazing incidence wide-angle X-ray scattering (2D GIWAXS) patterns of the pristine p(g2T-TT) and p(g2T-TT):crown ether mixture films are shown in Fig. 1b–d and Fig. S1 (ESI†). As-cast polymer films showed a largely amorphous state, while the incorporation of 1 wt% 18C6 or 15C5 led to improved ordering of p(g2T-TT) chains without necessity of any thermal treatment (Fig. S1, ESI†). Annealing treatment at optimal 125 °C induced a clear increase in crystalline features compared to as-cast thin films, as evidenced by the sharpening and intensification of peaks in the GIWAXS 1D profiles (Fig. S2, ESI†). Consequently, all the OECTs developed in this study utilized thin films that were annealed at 125 °C. The addition of 1 wt% 18C6 (Fig. 1c) or 1 wt% 15C5 (Fig. 1d) to the p(g2T-TT) film resulted in a more pronounced peak at lower q_{xy} and q_z values. From the (100) peak, the polymer with crown ether produced longer lamellar distances and longer lamellar coherence lengths in the out-of-plane direction (Table S1, ESI†). These results suggest the formation of larger ordered domains of p(g2T-TT) due to the interaction between the polymer and crown ethers. It is known that the addition of crown ethers can enhance polymer crystallinity induced by phase separation.[27] A summary of the extracted peak values and calculated parameters from 1D GIWAXS profiles is provided in Table S1 (ESI†).

To investigate the water wettability and surface energy of the above-mentioned thin films, contact angle measurements (Fig. S3, ESI†) and calculations of surface energies (γ) based on the Owens–Wendt method were conducted.[28] The experimental surface energies of pristine p(g2T-TT), 18C6-mixed p(g2T-TT), and 15C5-mixed p(g2T-TT) were calculated to be 31.2, 40.4, and 22.4 mN m^{-1}, respectively (Table S2, ESI†). Compared to the pristine p(g2T-TT), the 18C6-mixed p(g2T-TT) film displayed a reduced water contact angle and a higher surface energy. This was due to the increased hydrophilicity mainly caused by the 18C6 incorporation. On the other hand, the 15C5-mixed polymer film showed a higher water contact angle and lower surface energy, suggesting that the hydrophilicity/hydrophobicity and surface energy of the semiconducting layer are tuned by the crown ethers and that the 15C5-mixed film hinders electrolyte penetration. The observed differences may be mainly due to the difference in the ring size between 18C6 and 15C5, which significantly affect ion affinity, interactions with water molecules and the polymer matrix, and hydrophilicity.[29]

2.2 Basic performance of ion-selective OECTs

Next, the OECTs based on p(g2T-TT) or p(g2T-TT):crown ether mixture films as active layers were fabricated (Fig. 1a), and their

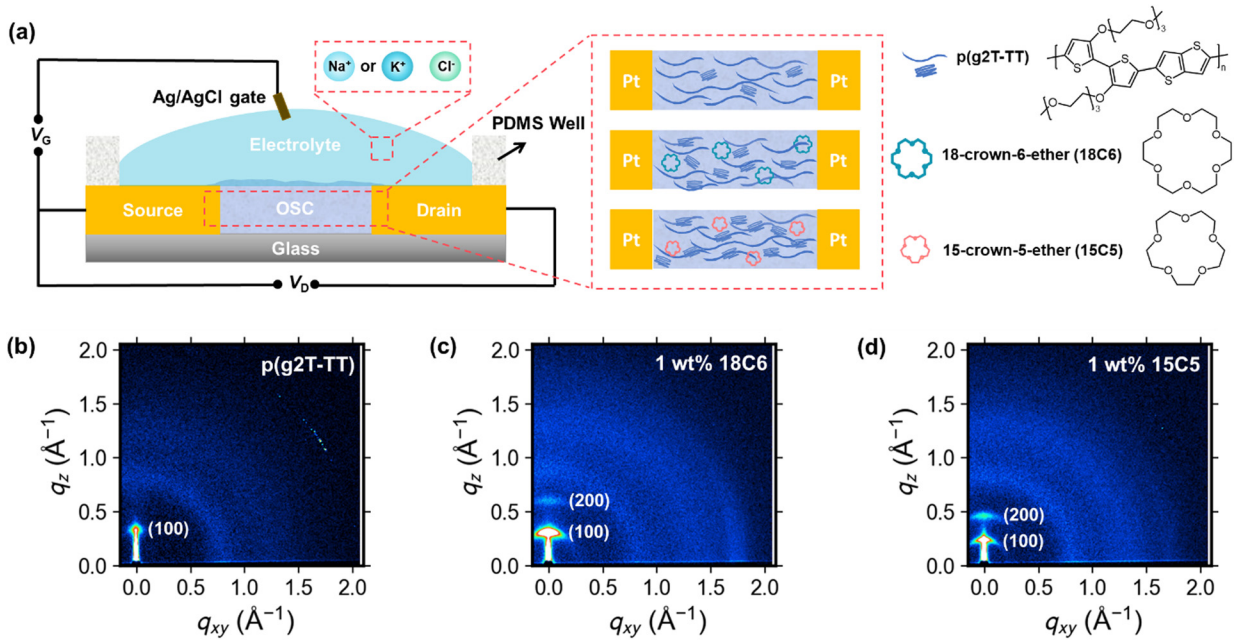

Fig. 1 (a) The schematic representation of organic electrochemical transistor (OECT) in this study with different active materials membrane: pristine p(g2T-TT); 18C6-mixed p(g2T-TT) and 15C5-mixed p(g2T-TT). The electrolyte in OECT was 0.1 M NaCl or KCl aqueous solution. Comparison of grazing incidence wide-angle X-ray scattering (GIWAXS) 2D patterns of polymer thin films after annealing at 125 °C for 10 minutes: (b) p(g2T-TT), (c) 1 wt% 18C6-mixed p(g2T-TT) and (d) 1 wt% 15C5-mixed p(g2T-TT).

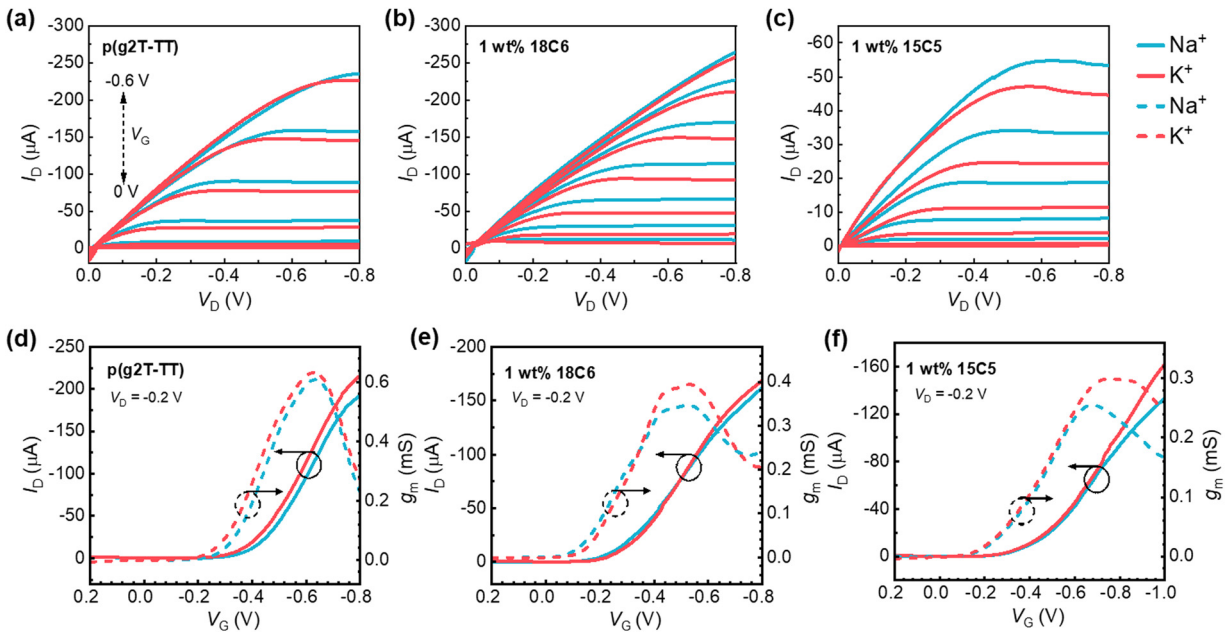

Fig. 2 Output and transfer characteristics of OECTs in the electrolyte of 0.1 M NaCl (blue) or KCl (red) aqueous solution: (a) and (d) pristine p(g2T-TT); (b) and (e) 18C6-mixed p(g2T-TT) and (c) and (f) 15C5-mixed p(g2T-TT).

electrical properties were evaluated. Fig. 2 shows the typical output curves, transfer curves, and transconductance (g_m, defined as the slope of the transfer curve: $\Delta I_D/\Delta V_G$) of the OECT with the electrolyte of 0.1 M of NaCl or KCl aqueous solution. By varying V_G from 0.2 to −0.8 V with V_D = −0.2 V, all the channel currents gradually increased to a saturated current state, indicating the successful p-channel accumulation operation behavior. Compared to the pristine p(g2T-TT) films, the blend film of 15C5 crown ether exhibited a lower channel current, which is consistent with the wettability change by adding crown ether. As shown in Fig. 2a and d, the OECT based on the pristine p(g2T-TT) showed no ion-selective behavior for Na^+ and

K^+ ions with similar drain current and transconductance. When p(g2T-TT):crown ether blend films were employed as channel materials, the higher transconductance values were observed for KCl than for NaCl as the gate voltage became more negative (−0.4 to −0.7 V for 1 wt% 18C6 mixed p(g2T-TT) and −0.6 to −1.0 V for 1 wt% 15C5 mixed p(g2T-TT)). This result clearly suggests Na^+/K^+-selective characteristics.

To further understand the effect of the crown ethers on the electrical properties, the concentration dependence of metal cations on the threshold voltage (V_{th}) and g_m in transfer characteristics was studied and the data are summarized in Fig. 3. The incorporation of the crown ethers into the p(g2T-TT) matrix resulted in a noteworthy reduction in the threshold voltage, V_{th} (absolute value), which can be attributed to several key factors. The selective ion-complexation capabilities of crown ethers alter the electrostatic environment within the polymer matrix, reducing the energy barrier for channel formation.[30] Additionally, as revealed by the GIWAXS patterns, the morphological changes by adding the crown ethers enhance polymer chain ordering, facilitate more efficient charge transport, and passivate the trap states, thus lowering the V_{th}. When a negative voltage is applied at the Ag/AgCl gate electrode, ionic polarization occurs in the electrolyte gate dielectric to accumulate hole carriers in p(g2T-TT). In the case of pristine p(g2T-TT), the Na^+ or K^+ ions in the electrolyte solution migrate toward the gate electrode to compensate for the electrode potential at the electrolyte/gate electrode interface. Simultaneously, the Cl^- ions penetrate into the p(g2T-TT) semiconductor layer and induce positive hole carriers in the transistor channel. As the electrolyte concentration gradually increases, more available Cl^- ions penetrate into the polymer matrix, resulting in a lower V_{th}. On the other hand, in the case of p(g2T-TT):crown ether blend films, the increase in the electrolyte concentration from 10^{-3} M to 1 M led to an increase in the V_{th}. This is due to the stronger interaction between the p(g2T-TT) and crown ether complex with Na^+/K^+ ions, leading to less effective charge screening by ions and requiring a higher gate voltage to induce conductivity.[31]

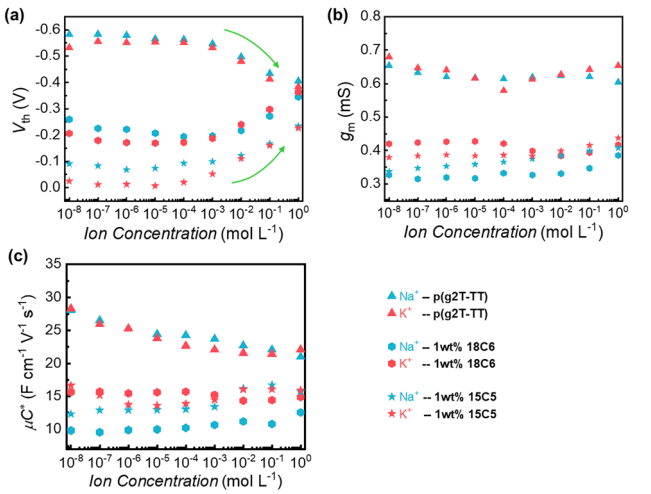

Fig. 3 Concentration dependence for (a) V_{th}, (b) g_m, and (c) μC^* in transfer characteristics. The results of p(g2T-TT) stand as triangle markers, hexagon as 1 wt% 18C6-mixed p(g2T-TT), and star as 1 wt% 15C5-mixed p(g2T-TT). Blue markers show the data obtained by using the NaCl aqueous solution as the electrolyte and the red ones by using the KCl aqueous solution.

Incorporating crown ethers into the p(g2T-TT) matrix led to a reduction in transconductance (g_m) (Fig. 3b). The g_m for pristine p(g2T-TT) approximately ranged from 0.6 to 0.7 mS, while the g_m decreased to approximately 0.3 to 0.4 mS by adding the crown ethers. The thickness of the pristine polymer film, 18C8 mixed p(g2T-TT), and 15C5 mixed p(g2T-TT), measured by atomic force microscopy (AFM), were 47 nm, 45 nm, and 38 nm, respectively. By applying the formula $g_m = (Wd/L)\mu C^*(V_{th} - V_G)$ for steady-state performance at saturation conditions in OECTs,[6] where W is the channel width, L is the channel length, d is the channel film thickness, V_G is applied gate bias, μ is the charge carrier mobility, and C^* is the volumetric capacitance, μC^* values were calculated and presented in Fig. 3c and Table S3 (ESI†). Thinner films generally exhibit reduced g_m due to surface effects, such as increased surface roughness and defects, which can trap charge carriers and reduce mobility.[7] The change in μC^* values suggests that the incorporation of crown ethers into p(g2T-TT) resulted in complex ion-polymer interactions and morphological changes that collectively reduce the effective mobility and transconductance.

2.3 Real-time cation detection and long-term operation stability

To further estimate the ion-selective performance in OECTs with channel materials of crown ether-mixed p(g2T-TT), how real-time OECT currents respond to a concentration reduction of Na^+ and K^+ ions in the electrolyte solution was evaluated and the results are shown in Fig. 4a–c. Differences in the ion-responsive performance were quantified by extracting and calculating the sensitivity of these two ions. Sensitivity is a key criterion for evaluating the detection capability of various biosensors. Here we employed a source–drain current difference (ΔI_D) to analyze the response performance of different ions and confirmed the validity of our findings, where $\Delta I_D = I_D^{Conc.} - I_D^{Conc.=C_0}$ ($I_D^{Conc.=C_0}$ is the source–drain current corresponding to the initial minimum concentration, and $I_D^{Conc.}$ denotes the source–drain current after decreasing the target ion concentration).[32] Accordingly, the related dose curves for each cation are presented in Fig. 4d–f. Such current responses to ion concentration were nearly instantaneous and do not require prolonged incubation of the device with the measurement solution.

As shown in Fig. 4a and d, the OECT with the pristine p(g2T-TT) channel exhibited no ion-selective behavior when gating with two types of aqueous electrolyte: NaCl and KCl (10^{-8} M to 1 M), which is in line with the results in Fig. 2. The sensitivity was proportional to the logarithm of the ion concentrations, which were extracted from the steady-state response after each injection. OECTs based on pristine p(g2T-TT) performed a similar I_D sensitivity in the linear range of 10^{-4}–1 M (10.63 μA dec^{-1} for Na^+; 10.45 μA dec^{-1} for K^+) and the limit of detection (LOD) (1.65×10^{-5} M for Na^+; 3.34×10^{-5} M for K^+) by applying these two different kinds of electrolytes (Table S4, ESI†).

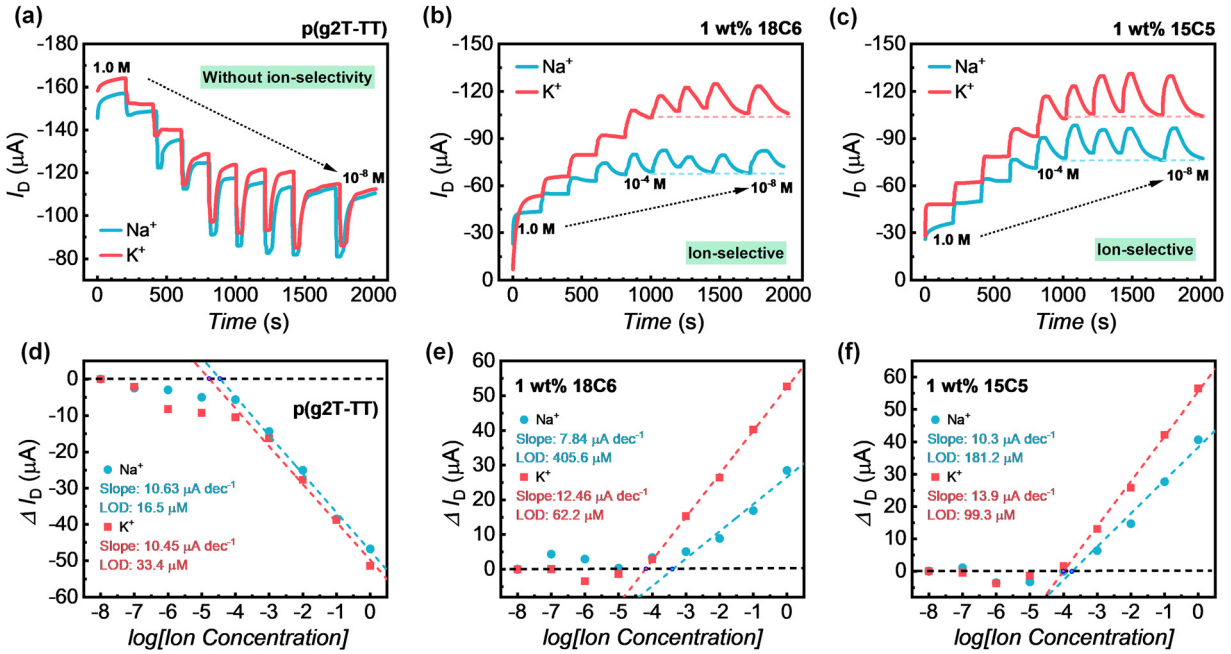

Fig. 4 Real-time cation detection using the studied OECTs and the response of the Na^+ and K^+ OECTs to a change in the electrolyte concentration (NaCl, blue; and KCl, red) from 1 M to 10^{-8} M (V_D = −0.6 V): (a) p(g2T-TT) at V_G = −0.6 V, (b) 1 wt% 18C6-mixed p(g2T-TT) at V_G = −0.5 V, and (c) 1 wt% 15C5-mixed p(g2T-TT) at V_G = −0.8 V. Calibration curves of the measured current at equilibrium to NaCl and KCl aqueous solutions with different concentrations: (d) p(g2T-TT), (e) 1 wt % 18C6-mixed p(g2T-TT), and (f) 1 wt% 15C5-mixed p(g2T-TT).

After incorporating the crown ethers into the polymer matrix, the ion-selective characteristics can be clearly observed, showing the higher drain-current response of K^+ ions (Fig. 4b and c). For 18C6-mixed p(g2T-TT), the sensitivity of the OECT for K^+ ions in the range of 10^{-4}–1 M was 10.63 μA dec^{-1} with LOD of 6.22×10^{-5} M. The device also responded to Na^+ ions, but the linear regime of the calibration curve was narrowed to the dynamic concentration range of 10^{-3}–1 M with a sensitivity of 7.84 μA dec^{-1} and LOD of 4.06×10^{-4} M (Fig. 4e). For 15C5-mixed p(g2T-TT), the sensitivity to K^+ was 13.9 μA dec^{-1} in the range of 10^{-4}–1 M, while its sensitivity to Na^+ was 10.3 μA dec^{-1} in the same linear range (Fig. 4f). Similar to the 18C6-mixed p(g2T-TT) sensor, the LOD of K^+ was lower than that of Na^+ for the 15C5-mixed p(g2T-TT) device. The parameters of the above discussion are summarized in Table S4 (ESI†). The performance of crown ether-mixed p(g2T-TT) OECT sensors for alkali-metal detection is compared with several ion-selective OECTs in Table 1. Compared to the other OECT sensors shown in Table 1, most of the OECTs required an additional membrane layer in the device configuration to achieve ion-selective detection technology. In this study, the membraneless detection of alkali metal ions was demonstrated in a simple way, and the developed OECT devices also exhibited a low detection limit and wide detection range.

Interestingly, the addition of crown ethers resulted in different current responses in the real-time concentration dependence measurements compared to the channel material with pristine p(g2T-TT) in OECTs (Fig. 4a–c). As the concentration decreased, the I_D of the pristine p(g2T-TT) device became progressively smaller, while the drain current of the crown ether-mixed channel gradually increased. The OECT based on p(g2T-TT) needed more than 50 s to reach a stable value, while the IS-OECTs based on crown ether-mixed polymers were stabilized within approximately 15 s at the range of 1–10^{-4} M, and the response time was independent of the ion concentration. At the same time, for IS-OECTs based on p(g2T-TT):crown ether system, the so-called current saturation period appeared in the range of 10^{-4}–10^{-8} M. Specifically, the I_D change showed an instantaneous increase at the moment the electrolyte concentration was changed, and such an instantaneous current was realized as the lower the concentration, the larger the current. Subsequently, the residual ions (such as Cl^-) in the channel gradually diffused or made a weaker contribution to the current, resulting in the observed gradual decrease in I_D. Finally, nearly identical equilibrium values were reached, and ion selectivity could be achieved even in such a detection range.

One of the major requirements for IS-OECTs detection is a stable operation of the active material. Therefore, after identifying the detection range and sensitivity of the sensors, the long-term operation stability of the IS-OECTs was evaluated (Fig. 5 and Fig. S4, ESI†). During this measurement, V_G was periodically turned on at −0.4 V for 5 seconds and turned off at 0 V for 5 seconds while maintaining V_D constant at −0.4 V. The I_D was recorded throughout the operation. As shown in Fig. 5a and c, the device based on pristine p(g2T-TT) and 1 wt% 15C5 mixed p(g2T-TT) exhibited extremely stable operational performance with 100% retention in NaCl aqueous solution. The stable operations were also demonstrated with no sign of degradation. However, in the OECT device based on 1 wt% 18C6 mixed p(g2T-TT) a slow device degradation was observed after 450 switching cycles (Fig. 5b), which aligns with the structural

Table 1 Comparison of ion-selective OECT performances for alkali-metal detection

Technology	Materials	Analytes	Sensitivity: Current ($\mu A\ dec^{-1}$)	Sensitivity: Voltage ($mV\ dec^{-1}$)	Linear range (M)	LOD (μM)	Fabrication	Year	Ref.
Electrolyte-gated OFET	ISM/P3HT	Na^+	—	62	10^{-6}–10^{-1}	1	Soft-molding/drop-casting	2013	33
Membraneless OECT	PEDOT:PSS/p(T15c5-ran-EDOT) or p(T18c6-ran-EDOT) electrode gate	Na^+, K^+	49	—	10^{-5}–10^{-1}, 10^{-3}–1	100	Photolithography/electropolymerization	2019	23
Microfluidics-integrated OECT array	ISM/PEDOT:PSS	Na^+, K^+	≈10	—	10^{-3}–10^{-1}	—	Inkjet printing	2020	34
IS-OECT	ISM/PSS:Na/PEDOT:PSS	Na^+, K^+	98, 224	—	10^{-4}–10^{-1}	9, 15	Photolithography/spin-coating	2020	17
OECT complementary amplifier	ISM/BBL/PEDOT:PSS	K^+	—	2344	10^{-5}–1	—	Photolithography/spin-coating	2020	35
Integrated IS-OECT	ISM/PSS:Na/PEDOT:PSS	Na^+, K^+	—	—	10^{-7}–10^{-3}	—	Photolithography/spin-coating	2021	36
IS-OECT	ISM/PEDOT:PSS with [MTEOA][$MeOSO_3$]	Na^+, K^+	312, 488	—	10^{-3}–10^{-1}	750, 800	Reactive ion etching/spin-coating	2022	18
IS-OECT	ISM/PSS:Na/PEDOT:PSS	Na^+	126	85	10^{-4}–1	110	Photolithography/spin-coating	2023	37
IS-OECT	ISM/PrC_{60}MA	Na^+, K^+	—	—	10^{-2}–1	0.1	Photolithography/spin-coating	2024	19
Membraneless OECT	**Ionophore mixed-p(2gT-TT)**	**Na^+, K^+**	**8–14**	—	**10^{-4}–1**	**≈18, 62**	**Commercial electrodes/spin-coating**	**This work**	

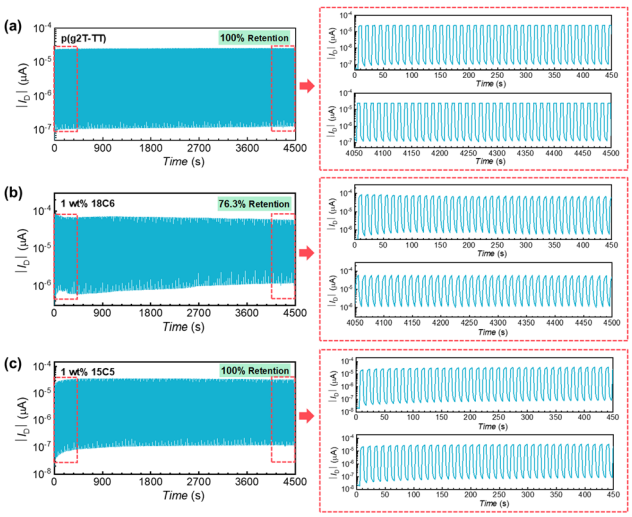

Fig. 5 Operational stability of drain current for OECTs. Transient responses of the drain current for V_D is −0.4 V and square pulse V_G switching between 0 and −0.4 V with the pulse width of 5 s for 450 cycles in 0.1 M NaCl aqueous solution. The right figures show the first 45 cycles (top) and the last 45 cycles (bottom): (a) pristine p(g2T-TT); (b) 18C6-mixed p(g2T-TT), and (c) 15C5-mixed p(g2T-TT).

insights from GIWAXS analysis. Upon addition of crown ether, the p(g2T-TT) polymer with 15C5-crown ether showed larger ordered crystalline domains than the case of 18C6-mixed p(g2T-TT), which is beneficial for better ion transport and interaction under different gate bias operation. The evaluation in KCl aqueous solution further reinforced these findings, where devices with 15C5-crown ether again showed good stability (Fig. S4, ESI†), showing 100%, 74.8%, and 97.8% retention performances for pristine p(g2T-TT), 1 wt% 18C6-mixed p(g2T-TT), and 1 wt% 15C5-mixed p(g2T-TT), respectively. Overall, the addition of 15C5-crown ether did not affect the stability of the polymer semiconductor, which showed an excellent long-term operational performance in both 0.1 M NaCl and KCl aqueous solutions. The comparison data of long-term stability measurements are summarized in Table S5 (ESI†).

2.4 Ion-selective proposed mechanism

In the case of pristine p(g2T-TT), the OECTs without crown ethers showed almost the same responses to changes in KCl and NaCl concentrations (Fig. 4a and d). According to the device physics, the I_D current of the p(g2T-TT)-based OECT depends on the anion injection.[6] As the electrolyte concentration gradually decreases, the I_D correspondingly decreases. Based on this analysis, the p(g2T-TT)-based OECT could not demonstrate ion selectivity for K^+ and Na^+. Additionally, the devices exhibited instability at the beginning of each cycle during injections, likely due to the high ionic strength of the solution.[34] On the other hand, as shown in Fig. 6b, since crown ethers and alkali metal ions can form supramolecular complexes, the crown ether incorporation into the semiconducting polymer matrix directly affects the I_D current in the channel. Specifically, taking exemplar 18C6-mixed p(g2T-TT), the incorporation of crown ethers caused phase separation between the polymer matrix and crown ethers (Fig. 1c and d). Hydration in the bulk of the polymer film and the swelling stage by ion injection could be facilitated. During the period of ion injection and exchange, cations (K^+) remain in the semiconductor channel because of their strong affinity to crown ethers. At the same time, since this kind of coordination compounds forms alkali metal cation–π interaction with the conjugated system, hole transport is hindered in the channel and accordingly the I_D current is lowered.[31] In the concentration-dependent ion selectivity test (Fig. 4b and e), as the electrolyte concentration decreased, the chloride concentration also decreased, directly reducing the conductivity of the channel. In this case, however, the polymers swelled and crown ether complexes were water-soluble. Therefore, the components of the system were further exchanged and diluted until the mass balance was restored.

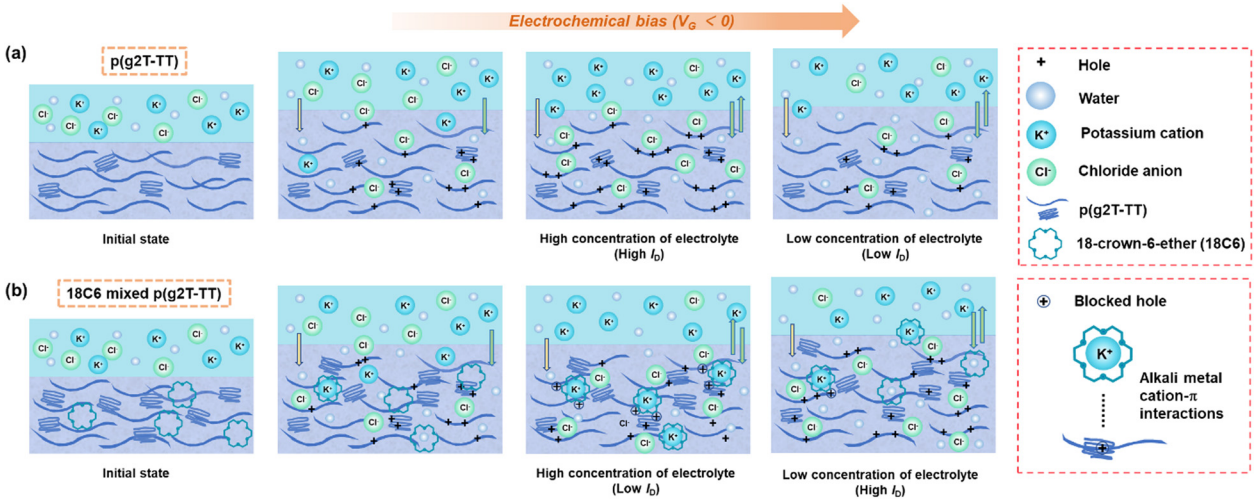

Fig. 6 Proposed mechanism of polymer doping process (polymer oxidation) based on (a) pristine p(g2T-TT) or (b) crown ether mixed polymer matrix (example of 18C6-mixed p(g2T-TT)), including the initial and swelling stages of the polymer film due to hydration and ion injection, the doping process in the presence of gate bias followed by conventional charge compensation *via* anion injection. The yellow arrows refer to the change in the polymer film volume (swelling); the green arrows correspond to the transport of charged species (injection/ejection).

This led to a weakening of the alkali metal cation–π interaction, which corresponds to the unblocking of holes in the polymer, thereby increasing the channel conductivity. Due to the synergistic effects of these factors, the I_D current of the IS-OECT increased as the concentration of the electrolyte solution decreased (Fig. 4b and c). Further investigation of the factors, such as the differences in the ion-complexation properties of Na^+ and K^+ with 18C6 or 15C5, variations in alkali metal cation–π interaction strengths with the conjugated polymer, and differences in the hydration capacity of the complexes, revealed that the OECTs with crown ether-mixed polymers exhibit ion selectivity for Na^+ and K^+ ions.[38,39]

3. Experimental section

3.1 Materials

The polymer semiconductor p(g2T-TT) was synthesized following a procedure previously reported in the literature as detailed in the ESI† (Scheme S1).[24] 18-Crown-6-ether (18C6) (TCI), 15-crown-5-ether (15C5) (TCI), sodium chloride (NaCl) (TCI), potassium chloride (KCl) (Fujifilm-Wako), potassium tetrakis-(4-chlorophenyl)borate (TCI) and chloroform (Sigma-Aldrich) were purchased from respective suppliers and used as received, without further purification. All aqueous solutions were prepared with ultrapure water (Millipore Milli-Q).

3.2 Polymer solution preparation

The p(g2T-TT) solution was prepared in chloroform at the concentration of 4 mg mL^{-1}. Blend solutions of 18C6-mixed p(g2T-TT) and 15C5-mixed p(g2T-TT) were prepared by incorporating 1 wt% of 18C6 or 15C5, along with 0.1 wt% potassium tetrakis(4-chlorophenyl)borate, into the p(g2T-TT) stock solution and these solutions were homogenized by stirring prior to thin film fabrication.

3.3 Characterization of polymer films

Two-dimensional grazing-incidence wide-angle X-ray scattering (GIWAXS) measurements were conducted at beamline BL40B2 in SPring8 (Hyogo, Japan). The X-ray beam had a wavelength of 0.1000 nm, with a camera length set to 111.0240 mm. The two-dimensional scattering image was captured using an Eiger2 S 500k photon counting detector (DECTRIS Ltd.). GIWAXS results were measured at the incident angle of 0.10°, which was lower than the critical angle of total external reflection at the silicon surface and was close to those of samples. The components of the scattering vector, q, parallel (q_{xy}) and perpendicular (q_z) to the sample surface, were distinctly defined. Thin film samples for GIWAXS measurements were prepared by spin-coating (2000 RPM/45 s) of the polymer solutions in chloroform onto $N^{++}Si/SiO_2$ substrate with/without annealing at 125 °C for 10 min. The thickness of annealed polymer films was examined by a Seiko Instruments SPA-400 with a stiff cantilever of Seiko Instruments DF-20. The samples for contact angle measurements were prepared by the same method as the GIWAXS sample fabrication. Static contact angles of the thin films were measured by the sessile drop technique using deionized water and glycerol as probe liquids with a surface electro optics Phoenix 150/300 contact angle analyzer. The surface energies were calculated based on the Owens–Wendt method.[28]

$$\gamma_{water}(1+\cos\theta_{water}) = \frac{4\gamma^d_{water}\gamma^d}{\gamma^d_{water}+\gamma^d} + \frac{4\gamma^p_{water}\gamma^p}{\gamma^p_{water}+\gamma^p} \quad (1)$$

$$\gamma_{glycerol}(1+\cos\theta_{glycerol}) = \frac{4\gamma^d_{glycerol}\gamma^d}{\gamma^d_{glycerol}+\gamma^d} + \frac{4\gamma^p_{glycerol}\gamma^p}{\gamma^p_{glycerol}+\gamma^p} \quad (2)$$

$$\gamma^{total} = \gamma^d + \gamma^p \quad (3)$$

3.4 OECT fabrication and characterization

The electrodes (10 nm Ti and 90 nm Pt) on a quartz glass substrate for the OECTs were sourced from BAS Inc. First, the above substrate was ultrasonically cleaned with deionized water, acetone and isopropanol, and then thoroughly dried by gas flow. Second, the prepared polymer solution was spin-coated onto the electrode-laden substrate at 2000 RPM for 45 s to form the thin films, which were subsequently annealed at 125 °C on a hot plate in air for 10 min. Finally, an Ag/AgCl electrode served as the gate electrode, with a PDMS well encasing the device channel. This configuration created a well-defined liquid area, isolating the solution from the source and drain electrodes. In this study, the channel dimensions were 100 μm in length and 10 μm in width. All electrical characterizations of the OECTs were conducted using a Keithley 4200A-SCS parameter analyzer in ambient conditions and ambient lighting. To obtain real-time current responses (I_D–time) with respect to the stepwise change in ion concentrations, the PDMS well was first placed on top of the substrate and filled with the original aqueous solution, and then I_D was recorded under constant V_G and V_D conditions. Once the baseline current was stabilized, the concentrations of Na^+ or K^+ were decreased by successively replacing the original aqueous solution by the subsequent corresponding NaCl and KCl solutions ranging from to 1 M to 10^{-8} M in the PDMS well.

4. Conclusions

In summary, the simple addition of crown ethers (15C5 and 18C6) to semiconducting polymers as channel materials has been successfully demonstrated as an efficient and straightforward method to fabricate the membraneless ion-selective (IS)-OECTs. The IS-OECTs in this study exhibited a higher current response to K^+ than to Na^+, demonstrating relatively high sensitivity and a low limit of detection. Notably, the IS-OECT based on 15C5-mixed p(g2T-TT) showed excellent stability with approximately 100% retention of performances. Finally, considering the device physics and substance interactions (*e.g.*, ion penetration and coordination interaction), an operating mechanism was proposed. The current study presents a simple and straightforward approach to modulate the electrical properties of conjugated polymers by utilizing crown ethers as additives in different sensor applications. The possibility of simply combining the ion-selective ionophores and a variety of functional materials with ionic-electronic transport functions opens up a broad range of prospects for future research.

Data availability

The data that support the findings of this study are available from the corresponding author upon reasonable request.

Author contributions

W. H.: investigation, data curation, formal analysis, and writing – original draft; Y. K.: investigation, data curation and formal analysis; N. N.: GIWAXS investigation; J. K.: data analysis and discussion; H. M.: GIWAXS investigation and discussion; Y. H.: supervision and discussion; T. M.: conceptualization, supervision, writing – review and editing.

Conflicts of interest

The authors have no conflicts of interest.

Acknowledgements

T. M. thanks the Nakatani Foundation for financial support. W. H. thanks Grant-in-Aid for JSPS Fellows (23KF0223). The synchrotron radiation experiments were performed at BL40B2 in SPring-8 with the approval of JASRI (Proposal No. 2023B1123). The authors thank Dr Hiroyasu Masunaga and Dr Noboru Ohta (JASRI) for assistance in the GIWAXS experiments.

References

1 M. Moser, J. F. Ponder, A. Wadsworth, A. Giovannitti and I. McCulloch, *Adv. Funct. Mater.*, 2019, **29**, 1807033.
2 A. Marks, S. Griggs, N. Gasparini and M. Moser, *Adv. Mater. Interfaces*, 2022, **9**, 2102039.
3 M. Sessolo, J. Rivnay, E. Bandiello, G. G. Malliaras and H. J. Bolink, *Adv. Mater.*, 2014, **26**, 4803–4807.
4 Y. Wang and Y. Liu, *Trends Chem.*, 2023, **5**, 279–294.
5 G. Liu, W. Wen, Z. Zhao, X. Huang, Y. Li, M. Qin, Z. Pan, Y. Guo and Y. Liu, *Adv. Mater.*, 2023, **35**, 2300242.
6 J. Rivnay, S. Inal, A. Salleo, R. M. Owens, M. Berggren and G. G. Malliaras, *Nat. Rev. Mater.*, 2018, **3**, 17086.
7 D. Ohayon, V. Druet and S. Inal, *Chem. Soc. Rev.*, 2023, **52**, 1001–1023.
8 A. Nawaz, Q. Liu, W. L. Leong, K. E. Fairfull-Smith and P. Sonar, *Adv. Mater.*, 2021, **33**, 2101874.
9 R. Kawamura and T. Michinobu, *Polymers*, 2023, **15**, 4657.
10 M. Y. Lee, H. R. Lee, C. H. Park, S. G. Han and J. H. Oh, *Acc. Chem. Res.*, 2018, **51**, 2829–2838.
11 A. Moudgil and W. L. Leong, *IEEE Sens. J.*, 2023, **23**, 8028–8041.
12 Y. Li, B. Cui, S. Zhang, B. Li, J. Li, S. Liu and Q. Zhao, *Small*, 2022, **18**, 2107413.
13 H.-S. Tseng, T. Puangniyom, C.-Y. Chang, J. A. Janardhanan, H.-H. Yu, W.-C. Chen, C.-C. Chueh and Y.-S. Hsiao, *Chem. Eng. J.*, 2024, **486**, 150371.
14 E. Bakker and E. Pretsch, *Anal. Chem.*, 2002, **74**, 420 A.
15 G. A. Crespo and E. Bakker, *RSC Adv.*, 2013, **3**, 25461.
16 C. Bieg, K. Fuchsberger and M. Stelzle, *Anal. Bioanal. Chem.*, 2017, **409**, 45–61.
17 S. Han, S. Yamamoto, A. G. Polyravas and G. G. Malliaras, *Adv. Mater.*, 2020, **32**, 2004790.

18 T. Li, J. Y. Cheryl Koh, A. Moudgil, H. Cao, X. Wu, S. Chen, K. Hou, A. Surendran, M. Stephen, C. Tang, C. Wang, Q. J. Wang, C. Y. Tay and W. L. Leong, *ACS Nano*, 2022, **16**, 12049–12060.
19 C. Shi, X. Jiang, Q. Wang, X. Dong, C. Xiang, Z. Wang, L. Chi and L. Huang, *J. Mater. Chem. C*, 2024, **12**, 4484–4492.
20 N. Abramova and A. Bratov, *Sensors*, 2009, **9**, 7097–7110.
21 H. Tseng, M. Cucchi, A. Weissbach, K. Leo and H. Kleemann, *ACS Appl. Electron. Mater.*, 2021, **3**, 3898–3903.
22 G. W. Gokel, W. M. Leevy and M. E. Weber, *Chem. Rev.*, 2004, **104**, 2723–2750.
23 S. Wustoni, C. Combe, D. Ohayon, M. H. Akhtar, I. McCulloch and S. Inal, *Adv. Funct. Mater.*, 2019, **29**, 1904403.
24 A. Giovannitti, D. T. Sbircea, S. Inal, C. B. Nielsen, E. Bandiello, D. A. Hanifi, M. Sessolo, G. G. Malliaras, I. McCulloch and J. Rivnay, *Proc. Natl. Acad. Sci. U. S. A.*, 2016, **113**, 12017–12022.
25 Y. Dai, S. Dai, N. Li, Y. Li, M. Moser, J. Strzalka, A. Prominski, Y. Liu, Q. Zhang, S. Li, H. Hu, W. Liu, S. Chatterji, P. Cheng, B. Tian, I. McCulloch, J. Xu and S. Wang, *Adv. Mater.*, 2022, **34**, 2201178.
26 L. Gao, Q. Zhang, Y. Lai, M. Xie, C. Liu, D. Zhang, Y. Peng, L. Bai, M. Wu, L.-W. Feng, W. Huang, J. Yu and X. Yu, *Nano Energy*, 2024, **129**, 110062.
27 M. Stephen, X. Wu, T. Li, T. Salim, K. Hou, S. Chen and W. L. Leong, *Mater. Horiz.*, 2022, **9**, 2408–2415.
28 D. K. Owens and R. C. Wendt, *J. Appl. Polym. Sci.*, 1969, **13**, 1741–1747.
29 H.-J. Buschmann, R.-C. Mutihac and E. Schollmeyer, *J. Solution Chem.*, 2010, **39**, 291–299.
30 D. T. McQuade, A. E. Pullen and T. M. Swager, *Chem. Rev.*, 2000, **100**, 2537–2574.
31 E. S. Meadows, S. L. De Wall, L. J. Barbour and G. W. Gokel, *J. Am. Chem. Soc.*, 2001, **123**, 3092–3107.
32 T. Nicolini, S. Shinde, R. El-Attar, G. Salinas, D. Thuau, M. Abbas, M. Raoux, J. Lang, E. Cloutet and A. Kuhn, *Adv. Mater. Interfaces*, 2024, **11**, 2400127.
33 K. Schmoltner, J. Kofler, A. Klug and E. J. List-Kratochvil, *Adv. Mater.*, 2013, **25**, 6895–6899.
34 S. Demuru, B. P. Kunnel and D. Briand, *Adv. Mater. Technol.*, 2020, **5**, 2000328.
35 P. Romele, P. Gkoupidenis, D. A. Koutsouras, K. Lieberth, Z. M. Kovacs-Vajna, P. W. M. Blom and F. Torricelli, *Nat. Commun.*, 2020, **11**, 3743.
36 D. A. Koutsouras, K. Lieberth, F. Torricelli, P. Gkoupidenis and P. W. M. Blom, *Adv. Mater. Technol.*, 2021, **6**, 2100591.
37 X. Meng, T. Zou, M. H. M. Chan, D. T. M. Chan, A. C. O. Tsang, G. K. K. Leung, S. Zhang and P. K. L. Chan, *Adv. Sensor Res.*, 2023, **3**, 2300097.
38 K. D. Fong, J. Self, B. D. McCloskey and K. A. Persson, *Macromolecules*, 2021, **54**, 2575–2591.
39 H. Høiland, J. A. Ringseth and T. S. Brun, *J. Solution Chem.*, 1979, **8**, 779–792.